

Flux trajectory analysis of Airy-type beams

ÁNGEL S. SANZ*

*Department of Optics, Faculty of Physical Sciences, Universidad Complutense de Madrid
Pza. Ciencias I, Ciudad Universitaria 28040 Madrid, Spain
a.s.sanz@fis.ucm.es

Abstract: Airy beams are solutions to the paraxial Helmholtz equation known for exhibiting shape invariance along their self-accelerated propagation in free space. These two properties are associated with the fact that they are not square integrable, that is, they carry infinite energy. To circumvent this drawback, families of so-called finite-energy Airy-type beams have been proposed in the literature and, in some cases, also implemented in the laboratory. Here an analysis of the propagation of this type of structured light beams is presented from a flux trajectory perspective with the purpose to better understand the mechanisms that make infinite and finite energy beams to exhibit different behaviors. As it is shown, while the foremost part of the beam can be clearly and unambiguously associated with the well-known accelerating term, the rear part of the beam corresponds to a nearly homogeneous distribution of flow trajectories, particularly for large propagation distances. This is shown to be related with an effective transfer of trajectories between adjacent lobes (gradually, from the fore part of the beam to its rear part), which leads to smearing out the transverse flow along the rear part of the beam. This is sharp contrast with the situation found in ideal Airy beams, where trajectories belonging to a given lobe of the intensity distribution remain the same all along the propagation. The analysis is supplemented with an also trajectory-based description of Young's experiment performed with finite-energy Airy beams in order to provide a dynamical understanding of the autofocusing phenomenon observed with circular Airy beams.

1. Introduction

Airy beams are solutions to the paraxial Helmholtz equation known for exhibiting shape invariance while they undergo self-acceleration when propagating in free space. Since their experimental implementation by Christodoulides and coworkers [1], this peculiar type of structured light has awakened much interest at present because of its potential applications [2, 3]. Nonetheless, although they are receiving much attention within the field of optics, they were first proposed in the field of quantum mechanics. As shown by Berry and Balazs [4] by the late 1970s, Schrödinger's equation admits a type of non-diffractive solutions with its amplitude having the functional form of an Airy function (a formal derivation and proof of these solutions was provided twenty years later by Unnikrishnan and Rau [5]). Thus, leaving aside the phase accumulated with time of these solutions, their amplitude is preserved in time all along the propagation. Hence, the associated probability density (or the intensity distribution, in the case of light beams) remains shape invariant. Nonetheless, it is also seen that these amplitudes undergo a uniform acceleration with time (they are self-accelerating) without the action of any external potential, which apparently seems to challenge Ehrenfest's theorem. Obviously, this is only the price to be paid for keeping the shape invariance and no fundamental quantum law is violated, as it can readily be noticed when computing the average position, which turns out to be zero at any time (i.e., the average position does not undergo any acceleration).

As it was pointed out by Greenberger [6], arguing in terms of the equivalence principle, although there is no external action, this free system can be shown to be equivalent to a free falling one, which renders "a more physically transparent interpretation", quoting Greenberger himself. More specifically, he finds that these Airy functions are eigensolutions of the Schrödinger equation describing a particle acted by a uniform gravitational field, just like plane waves are

eigenfunctions when external fields are lacking. These solutions were actually discussed by Greenberger and Overhauser earlier on [7] in the context of the experiment performed by Collela, Overhauser, and Werner in 1975 (the so-called COW experiment) [8] to determine the action of the uniform acceleration of the Earth's gravitational field on the phase shift undergone by neutrons in a Laue-type interferometer. Interestingly, earlier on, considering a different approach, Gibbs showed [9] that the eigenvalues of a point-like particle falling under the action of gravity and bouncing upwards again off a flat surface with no energy losses were given precisely by the Airy function. Specifically, the eigenvalues of this so-called quantum bouncer are proportional to the corresponding positions of the nodes of the Airy function (measured with respect to $x = 0$) [9–11], which has been experimentally investigated by Nesvizhevsky and coworkers [12–14].

In the case of light, it is clear that interpretations cannot be regarded to the action of an external gravitational field. Yet, the idea of recasting and investigating the flow associated with Airy beams in terms of “bending” rays is rather appealing. To this end, it is quite enlightening the alternative picture of light diffraction summarized in Born's and Wolf's renowned “Principles of Optics” [15], where the typical wave picture is substituted by a series of wiggling rays bending in conformity with the wavy behavior displayed by the phase after finding a conducting half-plane. These results were published in 1952 by Braunbek and Laukien [16], taking as a basis the solutions provided to edge diffraction by Sommerfeld [17] and the flux lines method proposed by Braunbek [18] in analogy to the relationship of rays with constant phase surfaces in geometrical optics. This method was applied to Young's two slits by Prosser later on [19], and more recently it has also been generalized to include polarization [20–23]. These depictions of light showed a good correspondence with the outcomes obtained in the implementation of Young's experiment with single photons by Steinberg and his group about a decade ago [24], where the use of the so-called weak measurements [25, 26] allows the experimental measure of the transverse momentum distribution under paraxial conditions without suppressing the final Young-type fringes.

Thus, taking into account the above theoretical framework, here an analysis of the propagation of Airy beams is presented and discussed in terms of the associated trajectories or streamlines with the purpose to better understand the transverse energy flow that makes special this type of structured light, exploring both infinite and finite energy conditions. It is known that the shape invariance and self-acceleration displayed by ideal Airy beams is connected to the fact that they are not square integrable, that is, that they carry infinite energy. Hence, to circumvent this drawback, families of so-called finite-energy Airy-type beams have been proposed in the literature and, in some cases, also implemented in the laboratory. In this regard, the trajectory picture here provided is intended to render some clues on the underlying mechanism that makes them to differ from ideal Airy beams, on the basis of how energy flows in space rather than on considering a standard analysis of the properties of the corresponding angular spectrum. As it is shown, while the foremost part of the beam can be clearly and unambiguously associated with the well-known accelerating term, the rear part of the beam corresponds to a nearly homogeneous distribution of flow trajectories, particularly for large propagation distances. This is shown to be related with an effective transfer of trajectories between adjacent lobes (gradually, from the fore part of the beam to its rear part), which leads to smearing out the transverse flow along the rear part of the beam. This is sharp contrast to the situation found in ideal Airy beams, where trajectories belonging to a given lobe of the intensity distribution remain the same all along the propagation. The analysis is supplemented with an also trajectory-based description of Young's experiment performed with finite-energy Airy beams. This apparently simple model arises motivated by the autofocusing phenomenon observed with circular Airy beams [27, 28].

Accordingly, the work is organized as follows. The analysis of ideal infinite-energy Airy beams is provided in Sec. 2, while its counterpart in the case of finite-energy Airy beams is presented in Sec. 3. The analysis of Young-type interference with two counter-propagating Airy beams is

presented and discussed in Sec. 4. Finally, a series of concluding remarks are summarized in Sec. 5.

2. Infinite energy Airy beams

Consider a monochromatic scalar field propagating in free space under paraxial conditions. As is well known, its behavior along the transverse direction can be parameterized in terms of the coordinate along which its propagation takes place. Thus, if propagation mainly takes place along the z direction, then the transverse behavior can be specified by $\mathbf{r}_\perp = (x, y)$, on planes perpendicular to the z -axis. At each z value, the behavior of the field amplitude, henceforth denoted as $\Psi(\mathbf{r}_\perp, z)$, is described by the paraxial form of Helmholtz's equation,

$$i \frac{\partial \Psi(\mathbf{r}_\perp, z)}{\partial z} = -\frac{1}{2k} \nabla_\perp^2 \Psi(\mathbf{r}_\perp, z), \quad (1)$$

where $\nabla_\perp = (\partial/\partial x, \partial/\partial y)$ and $k = 2\pi n/\lambda_0$, with n being the refractive index of the medium and λ_0 the wavelength in vacuum. Since the aim of this work is the analysis of the effective flux transfer along the transverse direction (rotations in the transverse plane are disregarded), let us only consider one transverse coordinate. Thus, instead of Eq. (1), we consider

$$i \frac{\partial \psi(x, z)}{\partial z} = -\frac{1}{2k} \frac{\partial^2 \psi(x, z)}{\partial x^2}, \quad (2)$$

where ψ is used instead of Ψ to avoid possible misunderstandings. To further simplify notation, reduced dimensions will also be used in the formal analysis, specifically, $\tilde{x} = x/x_0$ and $\tilde{z} = z/kx_0^2 = \lambda_0 z/2\pi n x_0^2$, where x_0 refers to a transverse distance of interest. This change of coordinates allows to recast Eq. (2) as

$$i \frac{\partial \psi(\tilde{x}, \tilde{z})}{\partial \tilde{z}} = -\frac{1}{2} \frac{\partial^2 \psi(\tilde{x}, \tilde{z})}{\partial \tilde{x}^2}. \quad (3)$$

Regarding the numerical values for the above introduced parameters, as in Ref. [1], here $n = 1$, $\lambda_0 = 488$ nm, and $x_0 = 53$ μm . Accordingly, $\tilde{x} \approx 18.87x$ and $\tilde{z} \approx 27.65 \times 10^{-3}z$, with both x and z in mm.

As it was shown by Berry and Balazs [4], the only non-diffractive (non dispersive) solution to Eq. (3) takes the form of an Airy function [29],

$$\psi(\tilde{x}, \tilde{z}) = e^{i(\tilde{x} - \tilde{z}^2/6)\tilde{z}/2} Ai(\tilde{x} - \tilde{z}^2/4), \quad (4)$$

with

$$Ai(s) = \frac{1}{\pi} \int_0^\infty \cos\left(\frac{u^2}{3} + su\right) du, \quad (5)$$

which keeps shape invariance all along its propagation at the expense of being a non square integrable function. Furthermore, it can also be seen that the beam amplitude (4) exhibits a quadratic displacement with the longitudinal coordinate, z , along the transverse direction, x . That is, any point of the beam amplitude or the associated intensity can readily be referred to the input beam,

$$\psi(\tilde{x}, 0) = Ai(\tilde{x}), \quad (6)$$

by simply adding the quantity $\tilde{x}_d = \tilde{z}^2/4$ or, in terms of the physical dimensions, $x_d = \lambda_0^2 z^2/16\pi^2 n^2 x_0^3 \approx 10.13 \times 10^{-6} \text{ mm}^{-1}$. Interestingly, in spite of showing an evidently accelerated-like displacement, by using the definition (5), it can easily be seen that the average position of these beams vanishes, that is, it seems to be no influence on the average transverse flow of energy.

To better understand this apparently paradoxical aspect, let us determine the transverse energy flux [15], which reads as

$$j(\tilde{x}, \tilde{z}) = \text{Im} \left[\psi^*(\tilde{x}, \tilde{z}) \frac{\partial \psi(\tilde{x}, \tilde{z})}{\partial \tilde{x}} \right] = \frac{\tilde{z}}{2} Ai^2(\tilde{x} - \tilde{z}^2/4). \quad (7)$$

Taking into account that the flux can always be written in the form of a transport relation, as $j = vI$, where $I(\tilde{x}, \tilde{z}) = |\psi(\tilde{x}, \tilde{z})|^2 = Ai^2(\tilde{x} - \tilde{z}^2/4)$ is the beam intensity distribution and v refers to a drift or transport effective “velocity” field acting on I , we have

$$v(\tilde{x}, \tilde{z}) = \frac{d\tilde{x}}{d\tilde{z}} = \frac{\tilde{z}}{2}. \quad (8)$$

Accordingly, by integrating over \tilde{z} , we obtain a series of flow trajectories or streamlines that determine how the intensity, I , is transported along the transverse direction as the beam propagates along the z direction. These trajectories thus show a quadratic parametric dependence on \tilde{z} ,

$$\tilde{x}(\tilde{z}) = \tilde{x}(0) + \frac{\tilde{z}^2}{4}, \quad (9)$$

in correspondence with the quadratic displacement exhibited by the amplitude (4).

Physically, Eq. (9) means that any trajectory starting within the region delimited by two nodes of ψ (or, equivalently, two vanishing minima of the corresponding intensity), will remain confined between them at any subsequent value of z . In other words, there is no effective transfer of energy between adjacent regions of the beam, as all the flow lines (trajectories) remain parallel one another. This underlying hydrodynamical description thus explains why the Airy beam remains invariant all along its propagation, namely, because there is not effective transfer of flow; keeping the beam accelerated in its ahead (or backward) propagation, like a continuously falling particle, prevents this dispersion or diffraction [6]. To some extent, the infinite-reach of the rear part of the beam somehow “pushes” the foremost one in this increasingly longer and longer transverse displacement.

This behavior is better understood by inspecting Fig. 1, where the propagation of an infinite-energy (ideal) Airy beam, from $z = 0$ to $z = 30$ cm, is represented in terms of a density plot. The plot clearly shows how both nodes and maxima of the intensity distribution follow parabolic trajectories, making the whole pattern to undergo a net rightwards displacement of 0.912 mm at $z = 30$ cm (this is better seen by comparing the intensity distributions shown in the two panels on the right side). When the beam propagation is represented in terms of (flux) trajectories, here indicated by the set of white solid lines superimposed to the density plot, we note that there is no mixture of the flux corresponding to different lobes of the intensity distribution. In other words, the intensity confined within two nodes remains the same all along the propagation. To monitor the propagation, we have associated three trajectories to each of the nine secondary maxima preceding the principal maximum, while nine of them have been associated to this one, since it is much wider than the other. Among the nine trajectories associated with the leading lobe, the initial condition of one of them has been chosen at the position of the maximum (see black solid line). Although in this particular instance of an ideal Airy beam, this trajectories behaves like any other, note that under conditions of finite energy (see below) it will serve to detect how much the beam deviates from ideality and at which z this situation becomes relevant.

3. Finite energy Airy beams

Generating an ideal Airy beam requires an infinite amount of energy as it can readily be noticed from its flat angular spectrum. Note that the Fourier transform, $\tilde{\psi}$, of the amplitude (6) is

$$\tilde{\psi}(k_x) = \int_{-\infty}^{\infty} Ai(\tilde{x}) e^{-ik_x \tilde{x}} d\tilde{x} = e^{ik_x^3/3}, \quad (10)$$

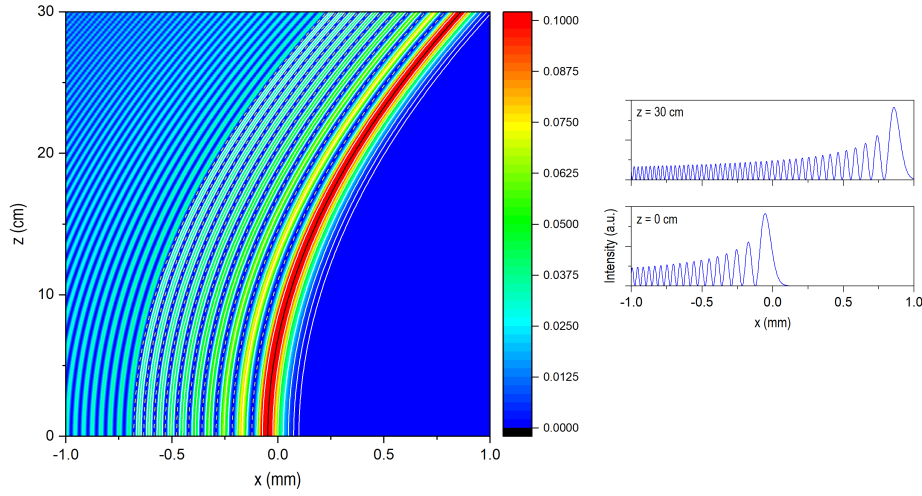


Fig. 1. Propagation of an infinite-energy Airy beam, from $z = 0$ cm to $z = 30$ cm. The density plot has been truncated at about 78% its maximum value in order to better visualize the evolution of the different secondary maxima and their gradual suppression. A set of flux trajectories is superimposed on the density plot in order to illustrate how the flux is channeled within adjacent zeros of the Airy function, without mixing with the flux associated with other lobes of the intensity distributions. To make these jumps more apparent, the evolution of the zeros of the ideal Airy beam has been denoted with orange dashed lines. The trajectory associated with the center of the principal maximum of the Airy beam is represented with a black solid line. In the right panels, input ($z = 0$ cm, bottom) and output ($z = 30$ cm, top) intensity distributions, normalized to the maximum value to better appreciate the details.

which is characterized by a unitary amplitude for all the transverse k_x components. A way to limit in extension the beam size, thus approaching more realistic working conditions (both in the laboratory and in numerical simulations), is by gradually suppressing the rear highly-oscillatory tail with a decaying exponential function (i.e., introducing an exponential-type aperture function), as indicated in [1]. Thus, considering

$$\psi(\tilde{x}, 0) = \text{Ai}(\tilde{x})e^{\gamma\tilde{x}}, \quad (11)$$

with γ positive and dimensionless, the propagated solution is given [1, 30] by

$$\begin{aligned} \psi(\tilde{x}, \tilde{z}) &= e^{i(\tilde{x}-\tilde{z}^2/6)\tilde{z}/2+\gamma(\tilde{x}-\tilde{z}^2/2)+i\gamma^2\tilde{z}/2} \text{Ai}(\tilde{x}-\tilde{z}^2/4+i\gamma\tilde{z}) \\ &= e^{i(\tilde{x}-\tilde{z}^2/6)\tilde{z}/2+\gamma(\tilde{y}-i\gamma\tilde{z}/2)} \text{Ai}(\tilde{y}), \end{aligned} \quad (12)$$

with

$$\tilde{y} = \tilde{x} - \tilde{z}^2/4 + i\gamma\tilde{z}. \quad (13)$$

Note that now the solution (12) represents a finite-energy Airy-type beam, with its amplitude determined by both a complex Airy function [29] [now $\text{Ai}^*(\tilde{y}) = \text{Ai}(\tilde{y}^*) \neq \text{Ai}(\tilde{y})$ for $\tilde{z} \neq 0$, which will eventually lead to a break of the shape-invariance that characterizes real-valued Airy-based solutions, as discussed below] and a modulating prefactor depending on the γ parameter. It is finite in energy, because the exponential term makes it to be a square integrable function, which can be seen through its angular spectrum [30],

$$\tilde{\psi}(k_x) = e^{-\gamma k_x^2 + i(k_x^3 - 3\gamma^2 k_x)/3 + \gamma^3/3}, \quad (14)$$

with a Gaussian amplitude. And it can be considered an Airy-type beam, because as long as γ remains small enough, the decay of the exponential term in (12) will be relatively slow and the solution will be close to an ideal Airy beam, exhibiting both shape invariance and self-acceleration. Of course, as γ increases, the deviation from an ideal Airy beam will be more evident, with the solution showing a gradual loss of its characteristic highly oscillatory features displayed beyond the main, leading maximum. This is a consequence of the asymptotic approach to a Gaussian type distribution, in compliance with the transverse momentum distribution described by (14).

Regarding the energy flux, it is clear that the presence of the imaginary component in the argument of the Airy function is going to play a crucial role, since now the Airy function becomes complex and hence it is going to actively contribute to j . In particular, after substitution of the wave function (12) into the first line of (7), we obtain

$$j(\tilde{x}, \tilde{z}) = \left\{ \frac{1}{2i} \left[Ai^*(\tilde{y}) \frac{\partial Ai(\tilde{y})}{\partial \tilde{x}} - Ai(\tilde{y}) \frac{\partial Ai^*(\tilde{y})}{\partial \tilde{x}} \right] + \frac{\tilde{z}}{2} Ai^*(\tilde{y}) Ai(\tilde{y}) \right\} e^{2\gamma(\tilde{x} - \tilde{z}^2/2)}, \quad (15)$$

which leads to the equation of motion

$$\begin{aligned} \frac{d\tilde{x}}{d\tilde{z}} &= \frac{1}{2i} \frac{\partial}{\partial \tilde{x}} \left\{ \ln \left[\frac{Ai(\tilde{y})}{Ai^*(\tilde{y})} \right] \right\} + \frac{\tilde{z}}{2} \\ &= \frac{\partial}{\partial \tilde{x}} \{ \arg [Ai(\tilde{y})] \} + \frac{\tilde{z}}{2}. \end{aligned} \quad (16)$$

Although Eq. (16) cannot be solved analytically, still some physical information of relevance can be extracted regarding the behavior of the flux. Comparing this equation of motion with Eq. (8), we find that, unless the first term in Eq. (16), on either line, becomes relevant, the behavior of the trajectories in this latter case is going to be similar to that exhibited by the trajectories associated with an ideal Airy beam. Accordingly, it is expected that the trajectories related to the foremost part of the beam will be less affected (or affected at longer values of \tilde{z}) than those in the rearmost part, where phase variations can be more dramatic. In the former case, the trajectories will follow a parabola similar to the one described by Eq. (9), at least, until they eventually become affected by finiteness of the beam. On the other hand, regarding those trajectories in the rearmost part of the beam, note that the first term in Eq. (16) will be of particular relevance whenever the phase variations become important, which will be close to nodes. Note that Airy functions have only zeros along the negative real axis; as \tilde{z} increases, though, these zeros move to the right, towards the region of positive \tilde{x} . However, the dependence on the imaginary term $i\gamma\tilde{z}$ is expected to cause a distortion of the positions of such zeros, thus provoking deviations from the parabolic motion and making the trajectories to get transferred from one lobe of the intensity to the adjacent one, just as in the case of Young-type interference [21].

To better understand the above statements, let us consider a numerical simulation based on the results presented and discussed in Refs. [1, 30]. The results from such simulation are shown in Fig. 2, where, as in the case of Fig. 1, a density plot of the finite-energy Airy beam has been represented with a set of trajectories superimposed with the purpose to show how the flux propagates with z . In this case, both the propagation of the beam and the synthesis of the trajectories have been numerically computed by means of an ad hoc prepared beam propagation method based on the split operator technique and an spectral Fourier expansion of the beam [31]. Unlike the ideal case, note that here there is an effective transfer of flux in the direction opposite to the transverse propagation, such that trajectories associated with a given lobe gradually “jump” to the adjacent ones. Such jumps take place whenever the trajectory crosses a minimum of the intensity distribution (note that these trajectories cannot cross nodes, but non-vanishing minima), where they undergo an important boost that allows them to keep propagating in the direction opposite to the transverse propagation. Thus, in the rear part of the beam we observe a trend towards a nearly homogeneous spatial distribution of the trajectories, as the intensity minima

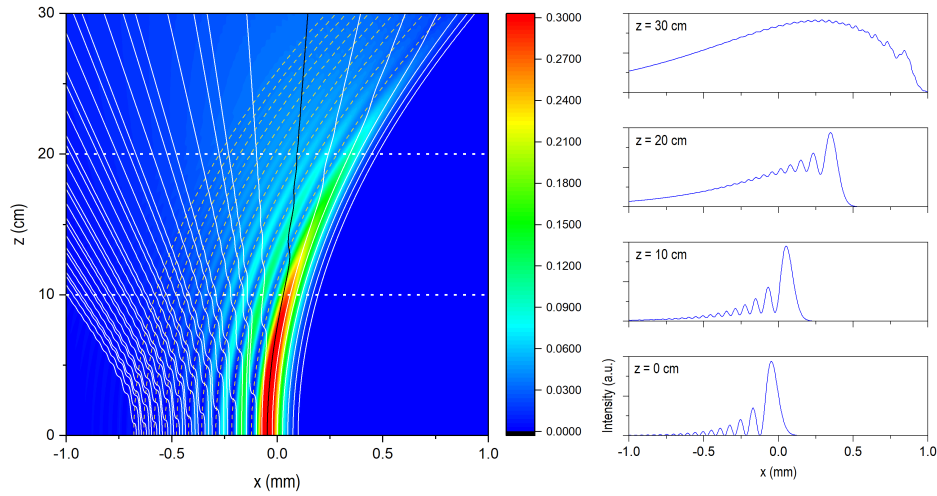


Fig. 2. Propagation of a finite-energy Airy beam with $\gamma = 0.11$, from $z = 0$ cm to $z = 30$ cm. The density plot has been truncated at about 78% its maximum value in order to better visualize the evolution of the different secondary maxima and their gradual suppression. A set of flux trajectories is superimposed on the density plot in order to illustrate how the flux jumps gradually from one secondary maximum to the adjacent one, in the direction from right to left. To make these jumps more apparent, the evolution of the zeros of the ideal Airy beam has been denoted with orange dashed lines. The trajectory associated with the center of the principal maximum of the Airy beam is represented with a black solid line. In the right panels, intensity distribution at different values of z , normalized to the maximum value to better appreciate the details, particularly at large values of z , where no relevant maxima are observed, but a monotonic trend to a Gaussian distribution centered at $x = 0$ mm. From bottom to top: $z = 0$ cm, $z = 10$ cm, $z = 20$ cm, and $z = 30$ cm. (For an easier identification, the central distributions correspond to the horizontal white dotted lines shown in the density plot.)

are gradually washed out [of course, with the proper weight the trajectory distribution should approach a Gaussian asymptotically, in agreement with the angular momentum distribution (14)]. On the other hand, regarding the leading lobe undergoes a gradual loss of trajectories with increasing z , losing the trajectory associated with its maximum (see black solid line) at about $z = 14$ cm. This is in correspondence with the intensity distribution profiles displayed in the panels on the right: while below $z = 10$ cm the beam can still be considered of the Airy type, at $z = 20$ cm nearly the main lobe and the adjacent one still remain, and at $z = 30$ cm an incipient asymptotic Gaussian-type distribution already starts becoming apparent. Nonetheless, the fact that a leading maximum can still be perceived is related to the fact that a few trajectories (related with a region of low intensity, as it can be noticed from the position of their corresponding initial conditions) keep track of the self-acceleration property.

4. Young's interference with finite energy Airy beams

Let us now consider the case of a coherent superposition of two finite Airy beams with the purpose to analyze the autofocusing in a one-dimensional model, which simplifies the dual autofocusing associated with circular Airy beams [27, 28] (the model in this work essentially corresponds to a transverse cut of one of such circular Airy beams). Given that the two beams are counter-propagating, following the behavior displayed by analogous two-beam superpositions, it

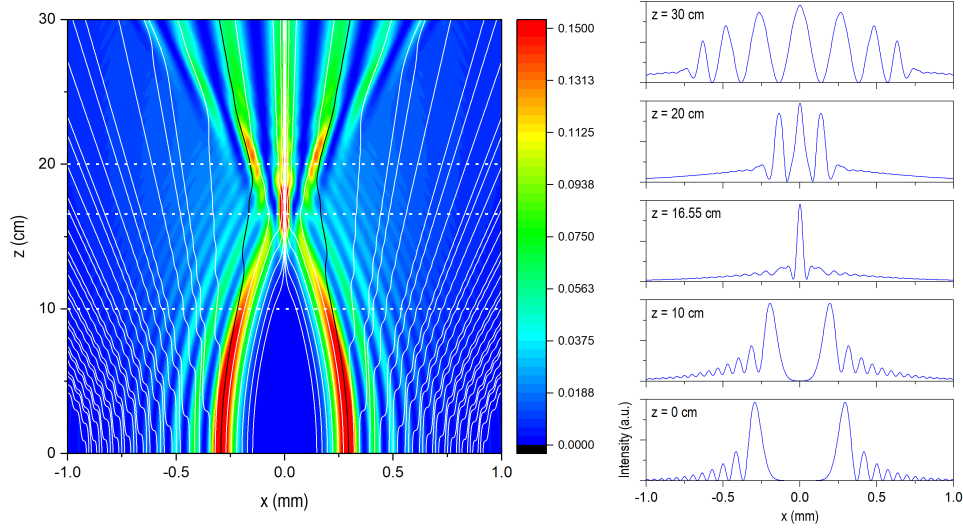


Fig. 3. Propagation, from $z = 0$ cm to $z = 30$ cm, of a superposition of two counter-propagating finite-energy Airy beams with $\gamma = 0.11$ and a peak-to-peak distance of about 0.6 mm. The density plot has been truncated at about 78% its maximum value in order to better visualize the evolution of the different secondary maxima and the emergence of the Young-type interference maxima after the merging of the two Airy beams. A set of flux trajectories is superimposed on the density plot in order to illustrate how the flux jumps gradually from one secondary maximum to the adjacent one, in the direction from right to left. Trajectories associated with the center of the principal maximum of each Airy beam are denoted with black solid lines. In the right panels, the intensity distribution at different values of z , normalized to the maximum value to better appreciate the details, particularly at large values of z , where no relevant maxima are observed. From bottom to top: $z = 0$ cm, $z = 10$ cm, $z = 20$ cm, and $z = 30$ cm. (For an easier identification, the central distributions correspond to the horizontal white dotted lines shown in the density plot.)

is clear that, at some point, Young-type fringes should emerge. Let us thus investigate the issue considering two identical counter-propagating solutions, each based on a spatial displacement of the input amplitude (11), namely,

$$\psi(\tilde{x}, 0) = Ai(\tilde{x} - \tilde{x}_0)e^{\gamma(\tilde{x} - \tilde{x}_0)} + Ai(\tilde{x} + \tilde{x}_0)e^{\gamma(\tilde{x} + \tilde{x}_0)}, \quad (17)$$

where the value of $\tilde{x}_0 = 0.246$ mm has been chosen to be equal to nearly the width of the leading lobe of a single Airy beam.

The results from the numerical propagation of the input beam (17), with $\gamma = 0.11$, are shown in Fig. 3, again in the form of a density plot with sets of trajectories superimposed on the regions covered by both merging beams (the initial conditions have been chosen as in the two previous cases analyzed, although with the corresponding spatial displacements on both sides with respect to $x = 0$). To the right, a series of panels show the profile displayed by the intensity distribution as z increases from the input plane to 30 cm, which stresses the fact that a prominent focused beam arises along the center of symmetry. Here, this focusing appears as a strong peak along the z axis, for about 5 cm, approximately. However, if we consider a full circular (finite energy) Airy beam instead, the addition of all contributions arising from the whole circle will lead to an even more prominent on-axis intensity concentration (with the model used here, such situation would correspond to an integration over a π angle around the z -axis). Beyond this region along z , we

already observe the emergence of a Young-type fringed intensity pattern, follow on both sides by a sort of smoothly decaying wings or tails, which is related to the fact that, far from the input plane, the structure of both beams is washed out, as seen in Sec. 3. Furthermore, also notice that, unlike conventional Young interference, here a gradual decrease in the width of each lobe is observed, which is related to the fact that the phase does not depend linearly with z . If, also here, we consider an integration around the z axis, it will be observed a higher accumulation of intensity along the axis, which is consistent with the autofocusing detected with circular Airy beams [27, 28]. When this behavior is translated in terms of trajectories (see solid white lines), we find that, if the corresponding trajectories start disseminating until $z = 15$ cm in the way described in Sec. 3, once the two beams abruptly merge the trajectories start self-organizing, rejoining within the newly formed intensity lobes. Moreover, in the merging, the fact that the “velocity” field relating the flux with the intensity is single valued (note that the beam local phase is single valued, except for a constant factor proportional to 2π) makes the trajectories to avoid their crossing along the axis, contrarily to what one might expect from usual geometrical rays. In this regard, because trajectories cannot cross, those corresponding to the centers of each leading maximum (see solid black lines) will not approach one another, but will bounce backwards until getting included within the respective second interference orders.

5. Concluding remarks

The use of geometrical rays is widely used to explain the behavior of optical phenomena, even if they involve a wave treatment of light, as it was formerly considered by Berry and Balazs [4]. Here, though, it has been shown that trajectories associated with the transverse flux of energy, in the manner originally proposed by Braunbek [16] and nicely summarized by Born and Wolf in their renown monograph [15], also constitute a suitable analysis tool, particularly to understand how the energy flows and hence to elucidate underlying differences between infinite and finite energy Airy-type beams. Specifically, it has been shown that, while the foremost part of finite-energy beams can be clearly and unambiguously associated with the well-known accelerating term, the rear part of the beam corresponds to a nearly homogeneous distribution of flow trajectories, particularly for large propagation distances. This has been shown to be related with an effective transfer of trajectories between adjacent intensity lobes (gradually, from the fore part of the beam to its rear part), which eventually leads to progressive a dissemination of the transverse flow along the rear part of the beam. This is in sharp contrast with the situation found in ideal Airy beams, where trajectories belonging to a given lobe of the intensity distribution remain the same all along the propagation. In sum, we have seen that the trajectories allow us to determine in a more quantitative manner (more than by simply inspecting the appearance of a density plot) which parts of the distribution are more importantly affected and how, or which ones are still in compliance with the self-acceleration that characterize ideal Airy beams.

Furthermore, we have also analyze the interference arising from a coherent superposition of two counter-propagating finite-energy Airy beams. Although it is not apparent from a standard density plot, the flux trajectories show a process of structure loss, denoted by the dissemination of trajectories, which jump from one intensity lobe to the immediately behind ones, one after the other, until the two leading maxima of the Airy beams coalesce on the same region along the z -axis. Then, the process reverts and the trajectories start reorganizing again, gathering along what seems to be a Young-type interference pattern, with an important accumulation of trajectories that move nearly parallel to the axis, thus explaining the emergence of autofocusing.

Funding This article has no associated award funding.

Disclosures The author declares no conflicts of interest.

Data availability All data generated and analyzed during this study are included in the presented research.

References

1. G. A. Siviloglou, J. Broky, A. Dogariu, and D. N. Christodoulides, "Observation of accelerating Airy beams," *Phys. Rev. Lett.* **99**, 213901 (2007).
2. N. K. Efremidis, Z. Chen, M. Segev, and D. N. Christodoulides, "Airy beams and accelerating waves: An overview of recent advances," *Optica* **6**, 686–701 (2019).
3. Y.-X. Ren, H. He, H. Tang, and K. K. Y. Wong, "Non-diffracting light wave: Fundamentals and biomedical applications," *Front. Phys.* **9**, 698343(1–30) (2021).
4. M. V. Berry and N. L. Balazs, "Nonspreading wave packets," *Am. J. Phys.* **47**, 264–267 (1979).
5. K. Unnikrishnan and A. R. P. Rau, "Uniqueness of the Airy packet in quantum mechanics," *Am. J. Phys.* **64**, 1034–1035 (1996).
6. D. M. Greenberger, "Comment on "nonspreading wave packets"," *Am. J. Phys.* **48**, 256–256 (1980).
7. D. M. Greenberger and A. W. Overhauser, "Coherence effects in neutron diffraction and gravity experiments," *Rev. Mod. Phys.* **51**, 43–78 (1979).
8. R. Colella, A. W. Overhauser, and S. A. Werner, "Observation of gravitationally induced quantum interference," *Phys. Rev. Lett.* **34**, 1472–1474 (1975).
9. R. L. Gibbs, "The quantum bouncer," *Am. J. Phys.* **43**, 25–28 (1975).
10. R. D. Desko and D. J. Bord, "The quantum bouncer revisited," *Am. J. Phys.* **51**, 82–84 (1983).
11. J. Gea-Banacloche, "A quantum bouncing ball," *Am. J. Phys.* **67**, 776–782 (1999).
12. V. V. Nesvizhevsky, H. Börner, A. M. Gagarski, G. A. Petrov, A. K. Petukhov, H. Abele, S. Bäßler, T. Stöferle, and S. M. Soloviev, "Search for quantum states of the neutron in a gravitational field: Gravitational levels," *Nucl. Instrum. Methods Phys. Res. A* **440**, 754–759 (2000).
13. V. V. Nesvizhevsky, H. G. Börner, A. K. Petukhov, H. Abele, S. Bäßler, T. S. F. J. Rueß, A. Westphal, A. M. Gagarski, G. A. Petrov, and A. V. Strelkov, "Quantum states of neutrons in the Earth's gravitational field," *Nature* **415**, 297–299 (2002).
14. V. V. Nesvizhevsky, A. K. Petukhov, H. G. Börner, T. A. Baranova, A. M. Gagarski, G. A. Petrov, K. V. Protasov, A. Y. Voronin, S. Bäßler, H. Abele, A. Westphal, and L. Lucovac, "Study of the neutron quantum states in the gravity field," *Eur. Phys. J. C* **40**, 479–491 (2005).
15. M. Born and E. Wolf, *Principles of Optics. Electromagnetic Theory of Propagation, Interference and Diffraction of Light* (Cambridge University Press, Cambridge, 1999), 7th ed.
16. W. Braunbek and G. Laukien, "Einzelheiten zur Halbebenen-Beugung," *Optik* **9**, 174–179 (1952).
17. A. Sommerfeld, "Mathematische Theorie der Diffraction," *Math. Ann.* **47**, 317–374 (1896).
18. W. Braunbek, "Zur Darstellung von Wellenfeldern," *Z. Naturforsch. A* **6**, 12–15 (1951).
19. R. D. Prosser, "The interpretation of diffraction and interference in terms of energy flow," *Int. J. Theor. Phys.* **15**, 169–180 (1976).
20. M. Davidović, A. S. Sanz, D. Arsenović, M. Božić, and S. Miret-Artés, "Electromagnetic energy flow lines as possible paths of photons," *Phys. Scr.* **T135**, 014009(1–5) (2009).
21. A. S. Sanz, M. Davidović, M. Božić, and S. Miret-Artés, "Understanding interference experiments with polarized light through photon trajectories," *Ann. Phys.* **325**, 763–784 (2010).
22. M. Božić, M. Davidović, T. L. Dimitrova, S. Miret-Artés, A. S. Sanz, and A. Weis, "Generalized arago-fresnel laws: The EME-flow-line description," *J. Russ. Laser Res.* **31**, 117–128 (2010).
23. M. Davidović, A. S. Sanz, M. Božić, D. Arsenović, and D. Dimić, "Trajectory-based interpretation of Young's experiment, the Arago-Fresnel laws and the Poisson-Arago spot for photons and massive particles," *Phys. Scr.* **T153**, 014015(1–5) (2013).
24. S. Kocsis, B. Braverman, S. Ravets, M. J. Stevens, R. P. Mirin, L. K. Shalm, and A. M. Steinberg, "Observing the average trajectories of single photons in a two-slit interferometer," *Science* **332**, 1170–1173 (2011).
25. Y. Aharonov, D. Z. Albert, and L. Vaidman, "How the result of a measurement of a component of the spin of a spin- $\frac{1}{2}$ particle can turn out to be 100," *Phys. Rev. Lett.* **60**, 1351–1354 (1988).
26. I. M. Duck, P. M. Stevenson, and E. C. G. Sudarshan, "The sense in which a "weak measurement" of a spin-1/2 particle's spin component yields a value 100," *Phys. Rev. D* **40**, 2112–2117 (1989).
27. N. K. Efremidis and D. N. Christodoulides, "Abruptly autofocusing waves," *Opt. Lett.* **35**, 4045–4047 (2010).
28. D. G. Papazoglou, N. K. Efremidis, D. N. Christodoulides, and S. Tzortzakis, "Observation of abruptly autofocusing waves," *Opt. Lett.* **36**, 1842–1844 (2011).
29. "NIST Digital Library of Mathematical Functions," <http://dlmf.nist.gov/>, Release 1.1.6 of 2022-06-30. F. W. J. Olver, A. B. Olde Daalhuis, D. W. Lozier, B. I. Schneider, R. F. Boisvert, C. W. Clark, B. R. Miller, B. V. Saunders, H. S. Cohl, and M. A. McClain, eds.
30. G. A. Siviloglou and D. N. Christodoulides, "Accelerating finite energy Airy beams," *Opt. Lett.* **32**, 979–981 (2007).
31. A. S. Sanz and S. Miret-Artés, *A Trajectory Description of Quantum Processes. II. Applications*, vol. 831 of *Lecture Notes in Physics* (Springer, Berlin, 2014).